Super Bowl, an open platform for visual stimulation of insects

Stefan Prech[1]*, Lukas N. Groschner[1,2], Alexander Borst[1]

1 Max Planck Institute for Biological Intelligence, Martinsried, Germany.

2 Present address: Gottfried Schatz Research Center, Medical University of Graz, Austria.

* stefan.prech@bi.mpg.de (SP)

Abstract

To study how the nervous system processes visual information, experimenters must record neural activity while delivering visual stimuli in a controlled fashion. In animals with a nearly panoramic field of view, such as flies, precise stimulation of the entire visual field is challenging. We describe a projector-based device for stimulation of the insect visual system under a microscope. The device is based on a bowl-shaped screen that provides a wide and nearly distortion-free field of view. It is compact, cheap, easy to assemble, and easy to operate using open source software for stimulus generation. We describe the general principle and test the system in a series of experiments measuring the membrane potentials of visual interneurons in the optic lobe of *Drosophila melanogaster*.

Introduction

Neural responses are inherently variable. The visual system is no exception in this respect, as repeated presentations of the same stimulus tend to elicit different neural responses. To decipher the influences of visual stimulation on neuronal responses, experimenters must be able to deliver light in a controllable and reliable manner. An ideal visual stimulation device would provide precise temporal and spatial control over every retinal photoreceptor cell. In recent years, research on the visual system of insects, in particular that of *Drosophila melanogaster*, has produced a rich collection of stimulation devices that take many shapes and forms. Fueled by technological advances, most of them either repurpose devices originally designed for the human visual system [1–5], or are custom-made from highly specialized components [6–9] rendering their implementation almost prohibitively expensive. To tailor a stimulation device to the demands of an insect's visual system, while keeping it versatile, compact and affordable, poses a formidable technical challenge.

In contrast to the human eye, the compound eye of *Drosophila* is tiled by hundreds of ommatidia arranged in a hexagonal grid. Each ommatidium of the convex retina collects light from a visual angle of approximately 5° [10] using a miniature lens with an aperture of 16 µm and a focal length of 20 µm [11,12]. These dimensions, for the most part, obviate the need to accommodate, as any object beyond a few millimeters appears at infinity focus. With an inter-ommatidial angle of ~5°, the spatial resolution of *Drosophila* is low, but the convex geometry of its eyes provides for a nearly panoramic field of view [13,14].

Dynamic visual environments for head-restrained insects that allow experimenters to record behavioral and neural responses to visual stimuli are commonplace in insect neuroethology [15]. Relicts of long-gone manufacturing constraints, most displays used to create these virtual environments have either a flat or a cylindrical geometry neither of which matches the shape of the fly eye. Hence, they all bear at least three caveats: First, they cover only a small fraction of the fly's field of view. Second, the brightness of the display varies across visual space as a function of the viewing angle; and third, distortions in the periphery of the visual field complicate the correspondence between actuator (pixels) and sensor (ommatidia) (Fig 1A–1C). While the latter two can be compensated for by computationally costly pre-adjustment and pre-distortion the displayed images, the first one is unavoidable.

Here, we describe an inexpensive projector-based visual stimulation device that caters to many of the demands of the insect visual system. It provides a wide and nearly distortion-free field of view with uniform brightness, but is compact enough to fit under a microscope. The crux of our system lies in its unconventional screen geometry, which simplifies both software and hardware development. Our open-source Python code allows any user with access to a computer and a 3D printer to create a bowl-shaped screen that suites the specifications (i.e. the throw ratio) of their projector. The temporal, spatial and spectral performance of the system can be adjusted, according to experimental requirements and budget constraints, by resorting to different commercially available projectors. We provide Python code to generate the screen design and to export it for 3D printing, but also to display a wide repertoire of visual stimuli commonly used by researchers, teachers, and students that study the insect visual system.

Results

Comparing screen geometries

We use a polyhedron as a simplified and general model of an invertebrate compound eye as a spherical approximation. As a simplified and general model of an invertebrate compound eye, we use a polyhedron as a spherical approximation. The screen capture from each projected polyhedron face can be understood as the number of projector pixels required to stimulate a certain fraction of the visual field, for example, one ommatidium or one spatial receptive field of a neuron. To allow direct comparison of different screen geometries, a Goldberg polyhedron—containing 272 almost identical faces—served as a model observer in front of a flat, a cylindrical, or a bowl-shaped virtual surface.

Observing the grid of a polyhedral projected onto a flat surface (Fig 1A), only the hexagon at the center of the visual field appeared undistorted. With increasing distance from the center, the hexagons grew rapidly in surface area and were increasingly distorted. At an angular distance of 50° from the center, hexagonal projections were on average 3.3 times longer and 1.9 times wider, after correcting for the hexagon's original aspect ratio; their area increased by a factor of 5.5. On a cylindrical surface (Fig 1B), hexagons remained undistorted along the equator but were subject to heavy distortions along the elevation axis. At an angular distance of 50° from the center, the average hexagon grew by a factor of 2.9 in elevation and 1.6 in azimuth. The area of a hexagonal projection increased by an average factor of 4.6. The bowl-shaped surface (Fig 1C) featured no distortion along the elevation and only slight azimuthal distortions in the periphery of the screen. At an elevation angle of 50° from the pole, the azimuthal distortion factor amounted to 1.2; at 100° from the pole, this factor was 2.4. The area of the hexagonal projection increased by the same factor of 1.2 at 50° and 2.4 at 100° from the center. Aside from robustness against distortions, a bowl-shaped screen features another advantage: It covers a substantially larger fraction of the visual field compared to a flat or a cylindrical screen of the same surface area. A cylindrical shape would require 44% of the area to cover the same visual field as a flat screen. The bowl-shaped screen can stimulate the same field of view with only 24% of the screen surface.

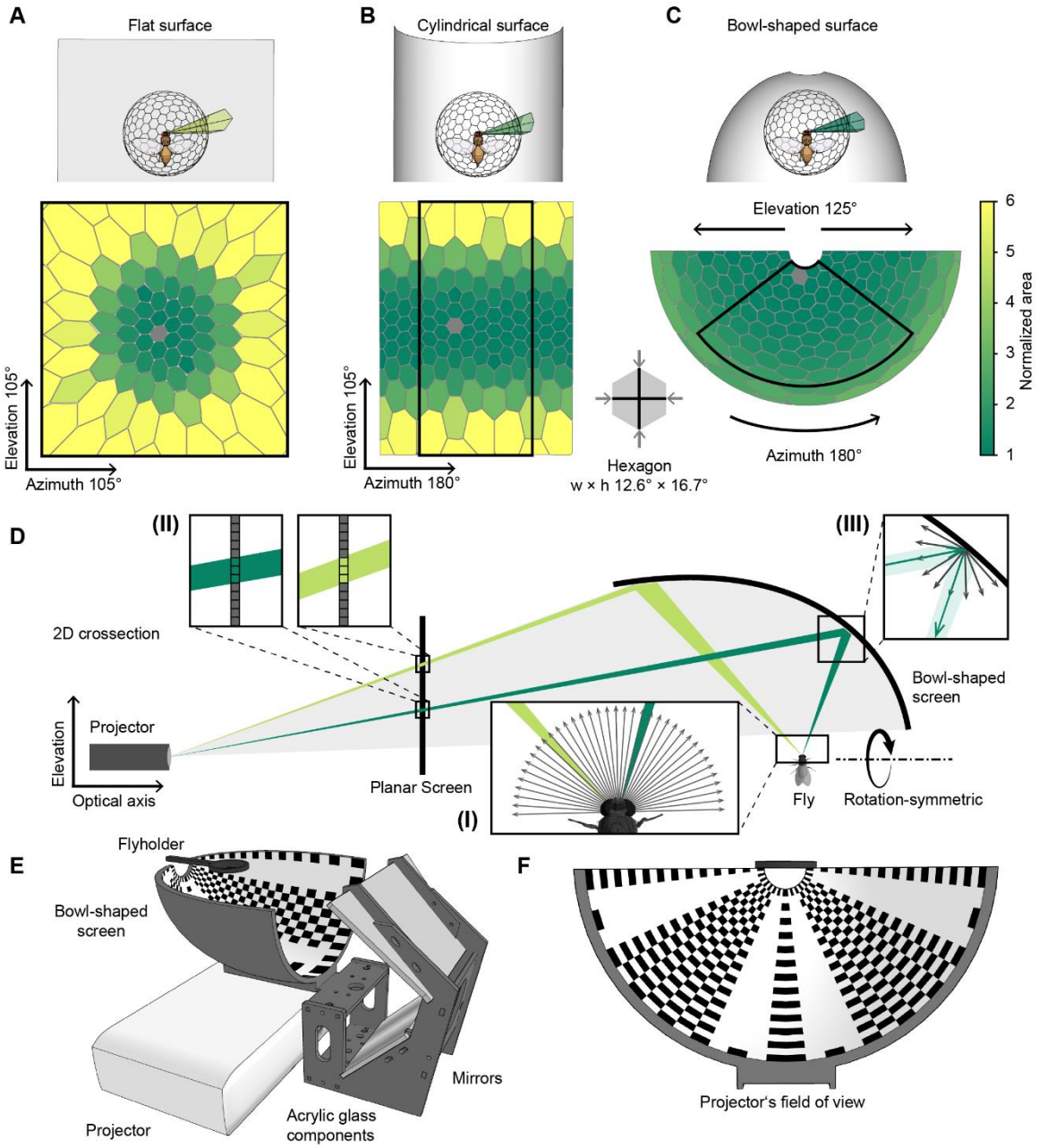

Fig 1: Geometry of the bowl-shaped screen
A-C Renderings of a virtual projection of a hexagonal grid onto a planar (**A**), cylindrical (**B**) and bowl-shaped surface (**C**). The area sizes are normalized to a standard undistorted hexagon at the center. One hexagon corresponds to the visual space covered by approximately nine ommatidia of *Drosophila melanogaster*. **D** Cross-section of the model used to calculate the screen geometry (Equation 3). (**I**) 2D spherical model to mimic the fly's photoreceptor arrangement, using a constant inter ommatidia angle of 5°. (**II**) 2D model of a projector which is designed to produce a uniform illumination and resolution on a planar screen. (**III**) Constant Lambertian reflection properties as well as the shape of the screen at any given point guarantee the homogeneous spatial luminance distribution. **E** View of the bowl-shaped screen, the mirrors and the projector. **F** The projector's field of view of the screen and the necessary equidistant azimuthal projection.

Screen design and evaluation

Our display system consists of an image projector and a screen. Like in any virtual reality system, the image must be pre-distorted in order to be accurately perceived from the position of the observer. Both the observer and the projector are stationary, which allows us to account for any perspectival distortions in a single step. The correction is not based on a computationally intensive software solution, as is usually the case, but on a hardware solution that uses a specific, pre-calculated screen geometry at no computational costs. To determine the ideal shape, we created simplified models of both the observer and the projector. A spherical model with a polar grid served as an approximation of the compound eye, where the optical axis of each ommatidium was represented by a radial vector connecting the center of the sphere with the center of the respective face. Taking advantage of the rotational symmetry of the sphere, we reduced the model of the observer to a two-dimensional cross section (Fig 1D I) (Equation 1). The projector model was simplified to the same extent by considering only two dimensions: one along the optical axis of the projector and a second one along the elevation (Fig 1D). Commercially available projectors are designed to project images with uniform pixel size and uniform luminance onto a planar screen (Fig 1D II) (Equation 2). To guarantee uniform brightness across the visual field of the insect, it is necessary to maintain a constant ratio of pixels (photons) per ommatidium of the convex retina (Fig 1D I). A precise correspondence between computer-generated pixels and the retinotopy of the insect visual system can only be established if this ratio is constant across the field of view. We implemented this by intersecting the optical axis vector of each ommatidium along the elevation plane with the modeled photon vector originating at the projector. The trajectory connecting the resulting intersection points defined the screen curvature along the elevation (Fig 1D) (Equation 3). The curvature of the screen along the azimuth was obtained by rotating the trajectory about the polar axis and interconnecting the trajectories (Equation 4). The resulting concave surface was predicted to be of uniform brightness, from the insect's point of view, provided that the screen surface features incidence angle-independent diffuse Lambertian reflectance (Fig 1D III). To achieve this property and to avoid artefacts caused by a cascade of specular reflection (Fig 2A), we coated the inner surface of the 3D-printed screen with different combinations of white paint and varnish. In order to test the optical properties of the surface, we illuminated square spots (5° × 5°) along the elevation and recorded the reflected light with a panoramic 360° camera (Fig 2B and 2C). One of these combinations showed almost no reflection along the elevation and was used in all subsequent experiments (Fig 2B and 2C).

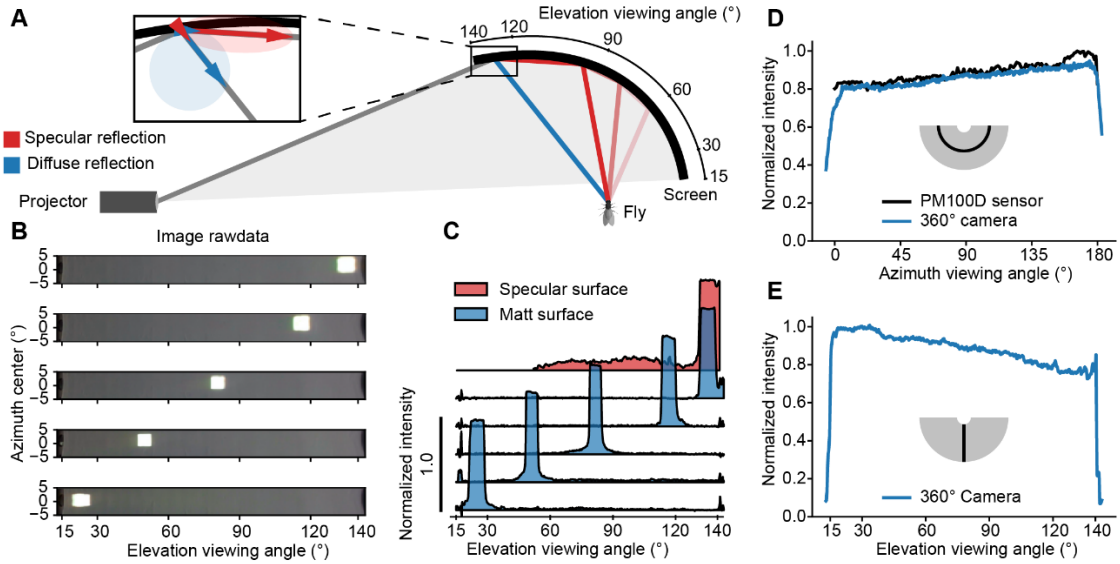

Fig 2: Technical validation of the operating principle
A Overview of Lambertian and specular reflectance properties of the screen surface. The blue vectors describe the diffuse, the red vectors the specular reflection component of an entering light ray. At flat angles of incidence, a reflective cascade is caused on the screens surface. **B** Raw image data of bright rectangular squares displayed at different locations along the elevation. **C** Cross-sections along the elevation of specular (red) and matte (blue) surfaces. The matte surface was evaluated at different locations along the elevation. In contrast to the matte surface, the specular surface (without coating) showed a pronounced reflection cascade. **D, E** Brightness profiles along the azimuth (**D**) and the elevation (**E**), measured with the 360° camera (blue). Measurements along the azimuth were controlled using an optical power meter (black).

Luminance measurements from the position of the observer using a rotatable power meter, as well as a 360° camera, corroborated our prediction and revealed an isotropic luminance across the entire elevation of the screen (Fig 2D and 2E). The calculated brightness uniformity (i.e., the lowest luminance reading at any point as fraction of the highest) amounted to 73%, which is comparable to the uniformity other projectors achieve on a planar screen, e.g., the DLP® LightCrafter™ Display 4710 EVM.

The bowl-shaped screen was held in place by acrylic glass components (Fig 1E). Two mirrors served to reduce the overall size of the set-up, but could be omitted depending on spatial constraints. In the present configuration, the mirrors allowed for the projector to be placed underneath the screen. In contrast to other virtual reality systems [1], the projector is easily replaceable and maintainable, making the system to the largest possible extent independent of the rapid product turn over on the consumer market. We used a standard projector with a native

resolution of 1280 × 720 pixels, a throw ratio of 1.4, a projection offset of 100% upwards, and an intrinsic brightness uniformity of ~90%. The projector has an image refresh rate of 60 Hz and a flicker frequency of 240 Hz, which exceeds the critical flicker fusion frequency of most insects including that of *Drosophila* [16]. Higher refresh rates could be achieved by using projectors like the ViewSonic® M2E (120 Hz) or the TI DLPLCR4500EVM (400 Hz).

Stimulus design and validation

In order to create an immersive, panoramic virtual reality for the animal, we take the insect observer to be at the center of a fictive unit sphere from where it observes an equidistant azimuthal projection of the sphere. Owing to the special geometry of the screen, this projection is—conveniently— identical to the image that must be displayed by the projector (Fig 1F). In other words, the screen geometry allows the direct projection of a spherical texture. The equidistant azimuthal projection is formally equivalent to a polar-transformed version of an equi-rectangular projection, the latter of which might be more familiar to the reader, for example, as a Cartesian map of the Earth. These interpretable equi-rectangular projections served as spherical textures and were chosen as the input format. In order to avoid subsequent interpolation, the projectors polar coordinate system was transformed into the cartesian coordinate system of the input texture using two pre-calculated transformation matrices: one for the x- and another for the y-coordinate of each pixel. The size of each matrix, and therefore the runtime, depends on the spatial resolution of the projector. Since the output image size, the transformation matrices, and the input image size were known (and constant) during runtime, we used just-in-time compilation within the JAX (Google) framework to calculate the transformations on the computer's graphics processing unit (GPU). On a standard laptop with a GTX1060 (Nvidia) graphics card, the transformation of a color image of 1280 × 720 pixels took on average 2-3 ms. Ahead of the transformation, to speed up processing times, equi-rectangular representations were cropped to the field of view covered by the screen (here, 180° × 125° in azimuth and elevation, respectively) and stimuli with a rotational component were pre-rotated (Fig 3B). To illuminate only the screen and to minimize stray light, a clipping mask was applied, which could be adapted to incorporate additions to the setup, such as time-stamp signals or cameras for monitoring behavior.

To put our stimulation device to a test, we placed a wide-angle camera (Fusion, GoPro) with a panoramic 360° field of view at the position of the observer. The camera provided a high-resolution equi-rectangular projection of the entire screen, which, given correct transformation and alignment, was expected to be identical to the input image. Comparison between the two allowed for a qualitative assessment of possible image distortions. As an input image, we used an equirectangular projection of the panorama from inside a cube with differently colored sides (Fig 3A) and inspected the transformed image at each step in the process chain: the cropped input image (Fig 3B), the projected image (Fig 3C), and the image captured by the 360° camera (Fig 3D). The cropped input image (Fig 3B) and the observed image (Fig 3D) were similar in terms of their proportions, grid geometry, contrast, sharpness, and field of view. This attests to the accuracy of the transformation and the correct, undistorted display of images on the 3D-printed screen.

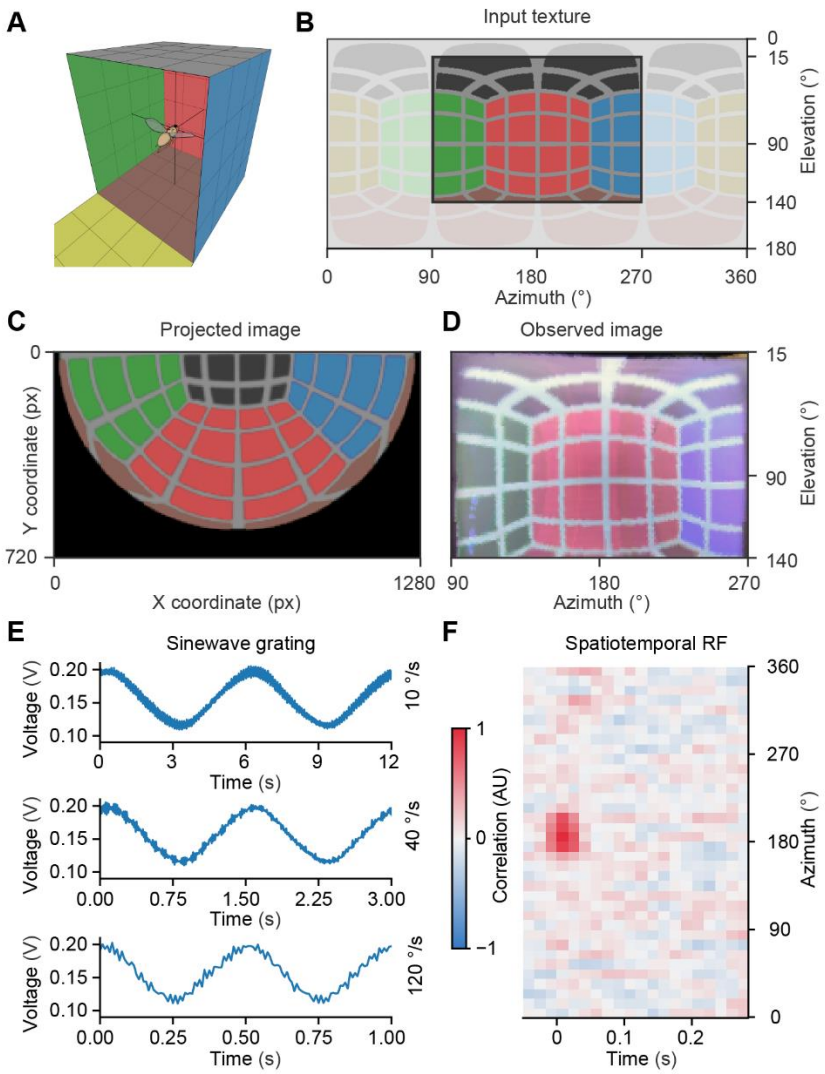

Fig 3: Technical validation of spatial and temporal stimulus control
A 3D view of the fly inside a virtual cube with colored walls. **B** Input image, an equidistant cylindrical projection of the virtual cube. The entire texture is shown in light color, the texture displayed by the screen is shown in dark color. **C** Texture from the viewpoint of the projector, prepared for being displayed on the bowl-shaped screen. **D** Captured image of the bowl-shaped screen from the 360° camera in equidistant cylindrical projection, the direct comparison to B. **E** Sinewave gratings moving at various velocities captured by a photodiode and resampled to a framerate of 120 Hz. **F** Spatiotemporal receptive field of the photodiode, measured over 8 minutes.

Time-varying visual stimuli were generated using custom-written software in Python. To quantify the temporal performance, rotational stimuli like sine wave gratings moving at various velocities (Fig 3E) as well as online generated stimuli such as discrete white noise stimuli (Fig 3F) were evaluated using a fast photodiode as a fly's proxy. In case of moving sine wave gratings, there were no conspicuous flickers in the down-sampled photodiode signal (<120Hz), which might be perceived by insects. Furthermore, the amplitude, the frequency and the phases were identical for all velocities (Fig 3E). The latter case shows that during a binary white noise stimulation period of 8 minutes at 60 Hz pattern change rate, a visible correlation in the temporal receptive field of the photodiode appeared only within the first 3 frames (50 ms). This suggests that, over a period of 8 minutes, jitter and drift are in the range ±1 frame (16.67 ms) (Fig 3F).

Experimental validation

The large, nearly distortion-free field of view and the uniform illumination of the bowl-shaped screen make it possible to stimulate the visual system in an identical manner at various spatial positions. This is essential, for instance, when spatiotemporal receptive fields of neurons at different spatial locations in the visual system are to be measured precisely. Before testing our bowl-shaped screen on real neurons, we measured the receptive field of a reference photodiode placed at different locations in the arena by projecting a 60 Hz spatiotemporal binary white-noise stimulus onto our screen. We cross-correlated the photodiode signal with the luminance at each screen position (Fig 4A) and corrected the resulting equirectangular image of the receptive field by rotating the position to the undistorted center of the cylindrical texture (Fig 4B). The result demonstrates that the perspective correction yields identical receptive field sizes, even in cases where the receptive field is located more than 50° off the center. The occurring deviations of about 8% were below the resolution of the binary white noise grid (Fig 4C).

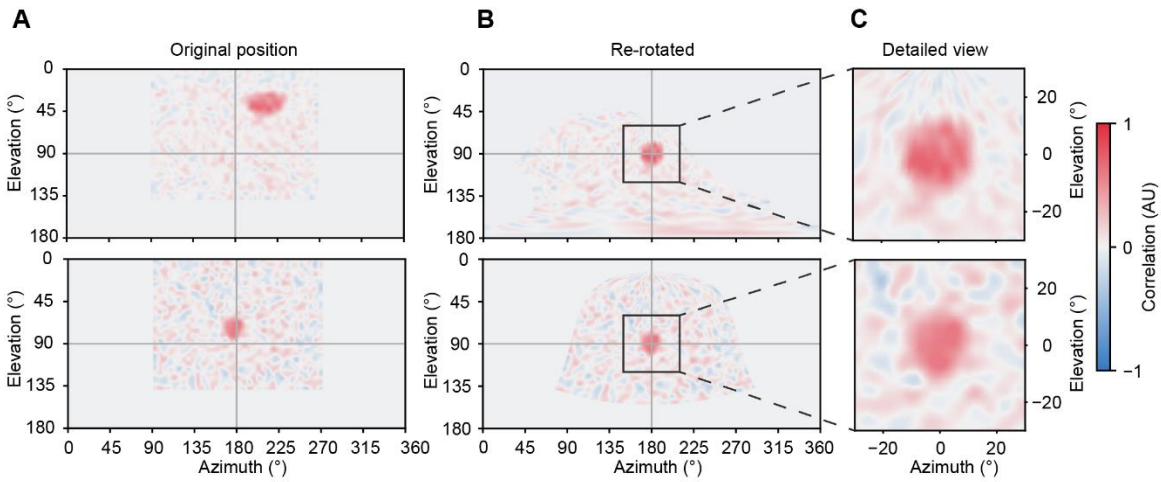

Fig 4: Technical validation of spatiotemporal receptive field measurements
A Equidistant cylindrical projection of the reverse correlation between input white noise and voltage signal of the photodiode. The "receptive fields" are displayed in their original positions. **B** Reverse correlation after the re-rotation into the distortion-free center of the equidistant cylindrical projection. **C** Detailed view of the "receptive fields" of the photodiode after re-rotation to allow direct comparison.

After the technical part, the biological validation was performed using *in vivo* patch clamp recordings of medulla intrinsic Mi9 neurons in tethered flies. First, we presented a 300-s binary white noise stimulus with a solid angle resolution of 2.8 degrees. The spatial center of mass of each receptive field was determined and corrected by inverse rotation, whereby the largest distance from the center was 38° in azimuth and 41° in elevation. We estimated the time-averaged spatial receptive fields at two different time intervals (0 to 0.1 s and 0.2 to 0.6 s) and the temporal linear kernel at the center of the spatial fields (Fig 5A). The full width at half maximum was ~10° (–3.5° to +6.5°) in azimuth and ~10° (–5.5 to +4.5°) in elevation, along both time intervals, and is consistent with previous measurements [17]. The temporal linear kernel shows a strong negative contrast correlation with a kernel density of ~–7 at 0.05 s and a weak positive correlation a with kernel density of ~1 at 0.57 s, which corresponds to a weak bandpass characteristic (Fig 5A). In addition, we tested a battery of commonly used visual stimuli: square-wave gratings and bright and dark edges moving at various velocities. The responses to moving gratings showed the expected frequency- and velocity-depended amplitude modulation (Fig 5B). The responses to moving bright and dark edges were aligned based on the location of the receptive fields position (Fig 5C). They show a mirror symmetric negative step response with respect to the stimulation contrast. In summary, the membrane potentials recorded from Mi9 neurons of flies stimulated using the bowl-shaped screen are consistent with those from an already established stimulation device [17,18].

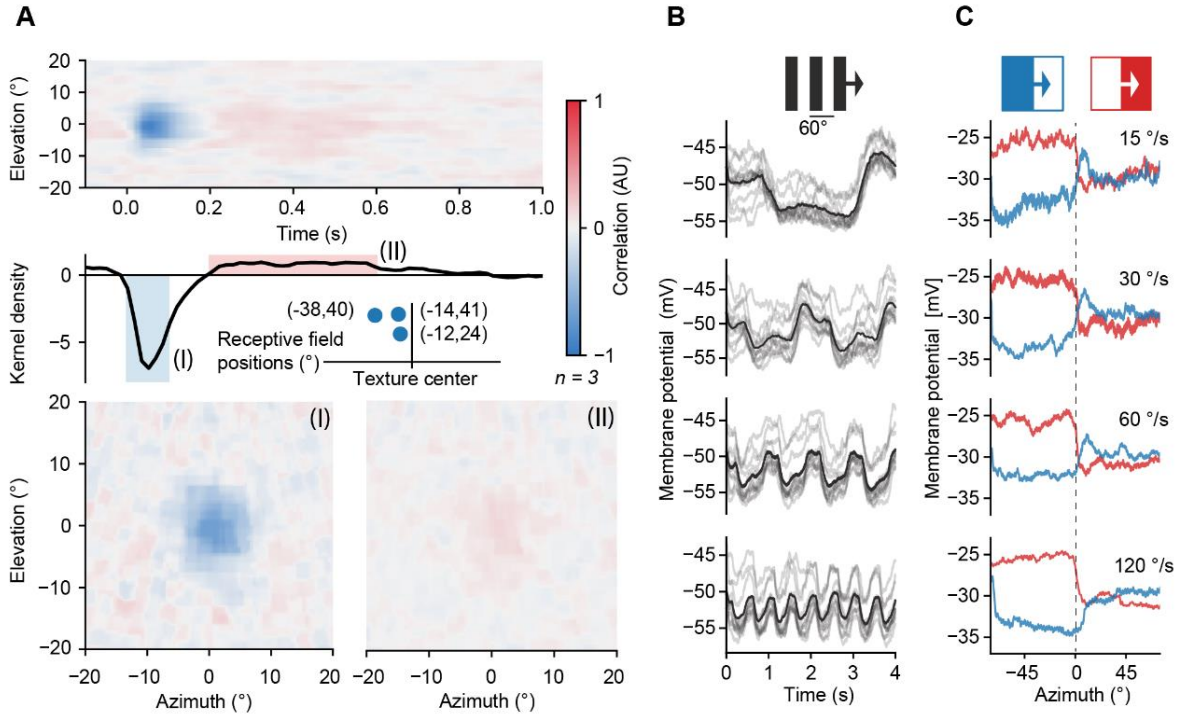

Fig 5: Voltage responses of medulla intrinsic Mi9 neurons to visual stimulation of the bowl-shaped screen

A Spatiotemporal receptive fields of three medulla intrinsic Mi9 neurons and their spatial position on the screen. Cross Section of the 3D kernel at the center of the azimuthal axis (top). Temporal kernel density estimation at the center of the spatial receptive field (center). Location of the centers of mass of the receptive fields on the screen (center). Spatial estimation of the correlation kernel in a time interval from 0 s to 0.1 s (**I**). Spatial estimation of the correlation kernel in a time interval from 0.2 s to 0.6 s (**II**). **B** Averaged (black) and single-trail (gray) membrane voltage responses of a Mi9 neuron (1 cell, 12 trails) to a 60°-wide horizontal square wave pattern, moving at four different velocities (15°/s, 30°/s, 60°/s, 120°/s). **C** Averaged Mi9 single cell voltage responses to bright and dark horizontal edges, moving at different velocities (15°/s, 30°/s, 60°/s, 120°/s) and aligned based on their receptive field positions (1 cell, 3 trails).

Discussion

The screen geometry of visual stimulation devices has important implications for the acquisition, the analysis, and the interpretation of functional data from the visual system. In many aspects, a cylindrical surface is superior to a flat one, but observer-related perspective distortions still remain. Super Bowl provides a virtual spherical texture, displayed on a spherical screen, virtually devoid of any projection-related distortions, which are otherwise difficult to overcome. The bowl-shaped screen geometry allows for a larger part of the visible space to be covered with far smaller distortions than in commonly used geometries.

All large system components, including the screen, can be 3D printed. The overall cost of the system depends on the type of projector used, which gives scientists a maximum of cost control. The system is compact and allows for recording neural responses under a microscope as well as for behavioral experiments. (Fig 1E and 6A). The distance of the projector and the size of the screen can be adjusted to the needs of the experiment. Thus, a complete immersive virtual environment can be created (Fig 6A). Alternatively, if required, a subset within the field of view can be stimulated selectively (Fig 6B). The system was designed to be easy to manufacture and assemble by scientists. The provided software generates vector graphic files that are readable by a broad range of programs and can be used as a design basis for 3D printing and laser cutting. The processes of filling and painting the screen require neither special equipment nor special practical skills. Projectors with identical throw ratios can be exchanged seamlessly, making it easy to incorporate the latest advances in spatial and temporal resolution. It should be mentioned, however, that the matte Lambertian surface is crucial for operation and the brightness distribution.

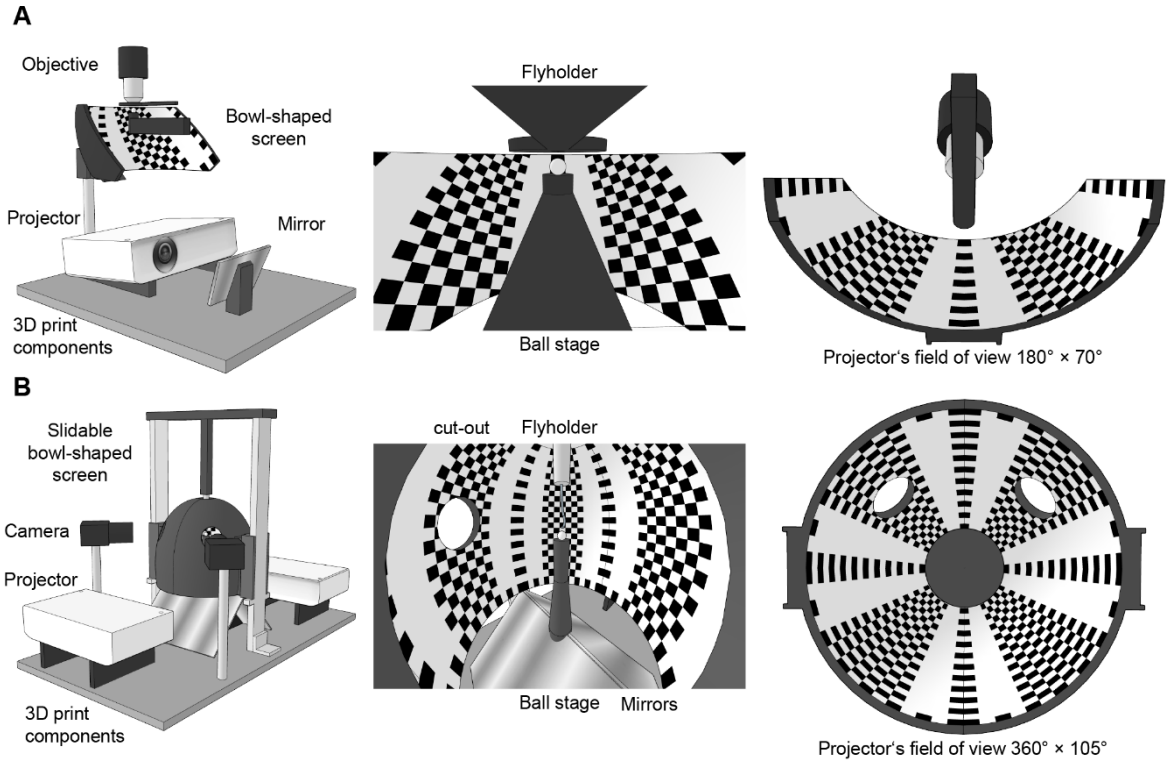

Fig 6: Application concepts of the bowl-shaped screen
A 3D rendering of a walking behaviour set-up, which also provides microscopic access to the brain. The field of view of the screen was designed in a way which enables closed loop bar fixation experiments, while recording neuronal activity. **B** 3D rendering of a fictive tethered walking behaviour setup, which creates an almost completely immersive virtual world around the fly. The system requires only two projectors and allows tracking cameras to be installed at various locations using cut-outs.

The included software for stimulus generation allows researchers and students to create visual stimuli and entire visual environments with ease. Accurately transformed projector output can be generated based on input from a game engine, a video, or a simple numeric array. The comparatively low computational demands of the software and fast online image transformation allow for the system to be used in closed-loop virtual reality settings. The self-written routines for transformation and rotation are easy to grasp and sufficient for most projectors. The performance can be increased if the calculation is carried out directly in a graphics library, like the Open Graphics Library (OpenGL).

Projector-based systems are compatible even with noise-sensitive electrophysiological experiments such as whole-cell patch clamp recordings (Fig 5). The only local source of electromagnetic noise, the power supply unit or the projector itself, can be easily shielded. Some projectors can be operated in battery-powered mode, increasing the versatility even further. Additionally, measuring spatiotemporal receptive fields in electrophysiological experiments is difficult in flat and cylindrical arenas. Receptive fields located in the periphery of the screen tend to be distorted and overestimated in size (Fig 1A and 1B) and moreover, because of their proximity to the edge, they often do not fully capture the surround of the receptive field. Therefore, it is common practice to include in the analysis primarily neurons with a receptive field at the center of the screen, which introduces a spatial picking bias and reduces the amount of analyzable data.

To investigate mechanisms of contrast normalization, especially the contribution of the visual surround on a neuron's receptive field [18–20], it is necessary to control luminance and contrast precisely across as much of the visual surround as possible. While the brightness of rear-projection screens [1,3,9] and conventional LED displays [5] depends on the viewing angle and requires adjustment at the cost of dynamic range, the bowl-shaped screen features nearly uniform brightness and only minimal perspective distortions. This allows for precisely measuring receptive fields of visual interneurons without the need to correct them post hoc, as is the case when using cylindrical or flat arenas.

A visual system with an almost panoramic field of view should be stimulated with the maximal possible field of view and as little distortion as possible, in order to fully understand its neurobiology. Although spherical wide-field displays have been used in behavioral

experiments [9], Super Bowl is the first spherical system that can stimulate a large field of view while recording nervous activity.

Materials and Methods

Assembly instructions and a user manual are available at:

https://github.com/borstlab/super_bowl_screen

https://www.youtube.com/playlist?list=PLcB8ZWnb7EzSwOxb3ipZU5DP4hZYWpbc6

Analytical solution of Super Bowl screen geometry

In two dimensions, the position of the fly is assumed to be at the center of the coordinate system, $Pos_{Fly} = \begin{bmatrix} 0 \\ 0 \end{bmatrix}$, and the position of the projector at a distance d_{proj}, i.e. $Pos_{Proj} = \begin{bmatrix} d_{proj} \\ 0 \end{bmatrix}$.

The throw ratio r_{throw} and the aspect ratio r_{aspect} are constants and can be summarized to $r = r_{throw} \cdot r_{aspect}$. A projection offset of 100% (projection upwards) is required. The elevation angle $\alpha \;\; with \; 0 < \alpha < \pi$ in radians is used to parameterize the bowl curve.

Thus, the viewing direction of the fly is given as

$$\overrightarrow{\mathrm{Fly}}(\alpha) = \begin{bmatrix} \cos(\alpha) \\ \sin(\alpha) \end{bmatrix}; \tag{1}$$

and the projecting direction of the projector is given as

$$\overrightarrow{\mathrm{Proj}}(\alpha) = \begin{bmatrix} 1 \\ \alpha/\pi \, r \end{bmatrix} + \begin{bmatrix} d_{proj} \\ 0 \end{bmatrix}; \tag{2}$$

The two vectors intersect at a point X, which has the coordinates:

$$\vec{\mathrm{X}}(\alpha) = d_{proj} \frac{\alpha}{\alpha - \pi \, r \, tan(\alpha)} \begin{bmatrix} 1 \\ \tan(\alpha) \end{bmatrix}; \tag{3}$$

The Vector $\vec{\mathrm{X}}(\alpha)$ determines the curve of the bowl-shaped screen along the optical axis and one axis perpendicular to it. To parametrize the surface area in $\mathbb{R}^3$, a second variable $\beta = \beta \in \mathbb{R}, \quad 0 < \beta < 2\pi$ is needed for the azimuth axis. The surface S of the bowl-shaped screen is then given by the outer product:

$$\vec{S}(\alpha,\beta) = d_{proj}\frac{\alpha}{\alpha-\pi\, r\, tan(\alpha)}\begin{bmatrix}1\\ \cos(\beta)\\ \sin(\beta)\end{bmatrix}\cdot\begin{bmatrix}1\\ \tan(\alpha)\\ \tan(\alpha)\end{bmatrix}^T. \quad (4)$$

3D modeling and printing

The screen shape along the elevation axis was calculated using a custom written script in Python v.3.7 (Python Software Foundation), using NumPy v.1.21.5, SymPy v.1.10.1, and Cairo v.1.16.0, based on the projector- and user-dependent input variables, such as distance, throw ratio, resolution, and field of view. Here, we specified a field of view ranging from 15° to 140° along the elevation axis. The automatically generated scalable vector graphics (SVG) file was imported into the computer-aided design program SketchUp (Trimble), where a 180° rotational extrusion along the optical axis of the path generated the final screen shape as a 3D surface mesh. After adding mounting connections to the drawing, a surface tessellation lattice (STL) file was exported for 3D printing. The screen was printed from black polylactide using fused filament fabrication on a Replicator 3D printer (MakerBot). Where a 3D printer is not available, online services such as Hubs (www.hubs.com), Materialise (www.materialise.com), Shapeways (www.shapeways.com), or Sculpteo (www.sculpteo.com) can be used to create the screen at competitive prices. Grooves in between filaments were filled using 2K General Purpose Body Filler (3M) to create a smooth texture. The surface was sanded and painted with three layers of white paint (585036, Dupli Color). To reduce specular reflection and associated artifacts, a final layer of matte varnish (Matt varnish 850, Marabu) was applied which is a critical step to achieve near-Lambertian reflective properties.

Assembly

The vector graphic of the beam path created in the previous step was also used as a guideline for the design of the holders. The dimensions and distances as well as the optical light field of the projection geometry were derived based on this. In order to minimize the overall dimensions of the system, we cut out and installed two planar metal-coated mirrors (ME8S-G01 - 8", Thorlabs) perpendicular to each other and at a 45° angle relative to the projector. Screen, projector, and mirrors were mounted on a frame made of matte black acrylic glass which was manufactured using a laser cutter (Speedy 360, Trotec). If a laser cutter is not

available, the frame can also be conventional manufactured, 3D printed or ordered from on-demand fabrication services (see above).

Stimulus generation

A custom build Python software was used to generate and project the stimuli, as well as to control the timing. For ease of use, the creation of stimuli is mainly done using the NumPy v.1.21.5 Python package, for rotating textures a “just in time compiled” function was written using the JAX package, to increase performance. As mentioned above, the projection function was also written using the JAX package. Software based image processing and presentation was realized using the OpenCV v.4.6.0 package. Timing was realized using the Python build in time module. After initialization, the software operates in a loop, which is run periodically with a stimulus dependent rate of 80 to 120 frames per second. Within each iteration, the elapsed time is determined and, based on this, a rotation or recalculation of the input texture is executed. The resulting texture is then projected, masked and displayed on the projector. This procedure continues until the stop time point is reached. The entire procedure can be processed in one thread; multithreading is not necessary, but would lead to additional speed-up. For closed-loop experiments, behavioral feedback can also be implemented in the stimulus generation or rotation pipeline.

The white noise stochastic stimulus used to determine the receptive fields, is updated online at 60 frames per second. The individual pixels correspond to a visual solid angle on a virtual equi-rectangular cylindrical texture. For example, using a solid angle of 5°, the field of view of the arena was divided into 36 × 28 pixels grid and the updating stimulus was displayed over 8 minutes. The intensities of the individual pixels were drawn randomly and were either 0% or 100% of contrast. Using a sliding reverse correlation, the impact of each stimulating pixel on the signal could be reconstructed. Each reconstructed image thus corresponds to an equidistant cylindrical projection of the receptive field.

Validation Measurements

To measure luminance profiles across the screen, we took two different approaches. First, we used a PM100D optical power meter (Thorlabs), whose sensor aperture was placed at the position of the observer. The angle of incidence was kept constant by rotating the sensor about

its axis using a servo motor (RS-2, Modelcraft) and a gimbal tracking the position of a square spotlight along the azimuth of the screen. In addition, we placed a 360° camera (Fusion, GoPro) with a resolution of 3000 × 3000 pixels at the position of the fly and took a photo of the scene in one shot. To obtain temporal high-speed measurements, we used a 5mm photodiode (L-7113GC, Kingbright) as a light sensor and acquired the voltage-signal generated by the photodiode by a 12 Bit digital Oscilloscope (WaveRunner HRO 66 zi, LeCroy).

Evaluation of screen geometries

To visualize the effect of screen geometry on the ratio of pixels per ommatidium, we generated computer-aided designs of a flat [2–4], a cylindrical [1,5], and a bowl-shaped screen (this paper). In place of the insect, we added a Goldberg polyhedron model of the observer. The polyhedron contained 260 hexagonal faces of equal area (±1%) and, like any Goldberg polyhedron, 12 pentagonal faces, each of which with an area of approximately 66% of that of the largest hexagon. On average, one hexagonal face covered a solid angle of 14°, equivalent to the angle covered by ~9 ommatidia of *Drosophila melanogaster*, a necessary approximation, given that Goldberg polyhedron cannot assume any arbitrary number of faces. Twenty of the hexagonal faces were regular, the rest were irregular hexagons with aspect ratios ranging from 0.87 to 1.07.

The edges of the faces were projected radially onto the screen surfaces, using the open-source physically-based render engine LuxCoreRender (https://luxcorerender.org). The resulting renderings were vectorized and analyzed in Python v.3.7.13. Hexagonal projections were color-coded based on their screen surface area relative to that of a central, undistorted projection. To allow for a rigorous comparison between the different structures, a field of view covering 105° in azimuth and elevation was considered for all screen shapes (Fig1A, B, C). For visualization purposes, we used an orthographic view of the flat screen and a flattened orthographic projection of the cylindrical screen. Additional perspective distortions that would occur in the cylindrical setting under real projection conditions were neglected. The projection of the bowl-shaped screen was already a perspective projection, which did not require additional image distortion.

Fly husbandry and genotypes

Flies were cultivated on a cornmeal, molasses and yeast medium under a 12 h–12 h light–dark cycle at 25 °C and 60% humidity. All of the experiments were carried out on female flies bearing at least one wild-type allele of the white gene. The experimenters were not blinded. Drosophila melanogaster of the following genotype were used to target transgene expression to the respective types of neuron: P{R48A07-p65.AD}attP40, P{10XUAS-IVS-mCD8::GFP}su(Hw)attP5; P{VT046779-GAL4.DBD}attP2 was used to label Mi9 neurons.

Patch-clamp recordings

Whole cell in vivo patch clamp recordings were performed as recently described [17]. In this procedure, female flies were cold-anesthetized 2-24 hours after hatching and fixed with soft thermoplastic wax on a special polyoxymethylene mount. The left dorsal optic nerve was exposed by surgical removal of the cuticle, adipose tissue, and trachea. Green fluorescent somata were visually identified by bright-field and epifluorescence microscopy. Using a small incision in the perineural sheath, access was provided to the cell membranes. Signals were recorded at room temperature (21-23°C) using a MultiClamp 700B amplifier, low-pass filtered, and sampled at 10 kHz. The data were corrected for the liquid junction potential and analyzed using custom-written Python software. The resting potential was determined to be the most negative membrane potential. Cells with a resting membrane voltage greater than -25 mV were excluded.

Funding

The Max Planck Society. Support for SP, LNG and AB. Horizon 2020 programme under the Marie Skłodowska-Curie Action MOVIS (grant agreement no. 896143). Support for LNG.

References

1. Arenz A, Drews MS, Richter FG, Ammer G, Borst A. The temporal tuning of the *Drosophila* motion detectors is determined by the dynamics of their input elements. Curr Biol. 2017;27: 929–944. doi:10.1016/j.cub.2017.01.051

2. Bahl A, Ammer G, Schilling T, Borst A. Object tracking in motion-blind flies. Nat Neurosci. 2013;16: 730–738. doi:10.1038/nn.3386

3. Creamer MS, Mano O, Tanaka R, Clark DA. A flexible geometry for panoramic visual and optogenetic stimulation during behavior and physiology. J. Neurosci. Methods. 2019;323: 48–55. doi:10.1016/j.jneumeth.2019.05.005

4. Loesche F, Reiser MB. An inexpensive, high-precision, modular spherical treadmill setup optimized for *Drosophila* experiments. Front Behav Neurosci. 2021;15: 689573. doi:10.3389/fnbeh.2021.689573

5. Reiser MB, Dickinson MH. A modular display system for insect behavioral neuroscience. J. Neurosci. Methods. 2008;167: 127–139. doi:10.1016/j.jneumeth.2007.07.019

6. Isaacson M, Ferguson L, Loesche F, Ganguly I, Chen J, Chiu A, et al. A high-speed, modular display system for diverse neuroscience applications. Neuroscience; 2022 Aug. doi:10.1101/2022.08.02.502550

7. Kócsi Z, Murray T, Dahmen H, Narendra A, Zeil J. The Antarium: A reconstructed visual reality device for ant navigation research. Front Behav Neurosci. 2020;14: 599374. doi:10.3389/fnbeh.2020.599374

8. Perkel JM. How remouldable computer hardware is speeding up science. Nature. 2021;600: 348–349. doi:10.1038/d41586-021-03627-8

9. Williamson WR, Peek MY, Breads P, Coop B, Card GM. Tools for rapid high-resolution behavioral phenotyping of automatically isolated *Drosophila*. Cell Rep. 2018;25: 1636-1649.e5. doi:10.1016/j.celrep.2018.10.048

10. Götz K. Optomotorische Untersuchung des visuellen Systems einiger Augenmutanten der Fruchtfliege Drosophila. Kybernetik. 1964;2: 77–92.

11. Stavenga DG. Angular and spectral sensitivity of fly photoreceptors. II. Dependence on facet lens F-number and rhabdomere type in *Drosophila*. J Comp Physiol A. 2003;189: 189–202. doi:10.1007/s00359-003-0390-6

12. Stavenga DG. Angular and spectral sensitivity of fly photoreceptors. I. Integrated facet lens and rhabdomere optics. J Comp Physiol A. 2003;189: 1–17. doi:10.1007/s00359-002-0370-2

13. Heisenberg M, Wolf R. Vision in *Drosophila*: Genetics of Microbehavior. Berlin: Springer; 1984.

14. Zhao A, Gruntman E, Nern A, Iyer NA, Rogers EM, Koskela S, et al. Eye structure shapes neuron function in *Drosophila* motion vision. Neuroscience; 2022 Dec. doi:10.1101/2022.12.14.520178

15. Dombeck DA, Reiser MB. Real neuroscience in virtual worlds. Curr. Opin. Neurobiol.. 2012;22: 3–10. doi:10.1016/j.conb.2011.10.015

16. Miall RC. The flicker fusion frequencies of six laboratory insects, and the response of the compound eye to mains fluorescent ‘ripple.’ Physiol Entomol. 1978;3: 99–106. doi:10.1111/j.1365-3032.1978.tb00139.x

17. Groschner LN, Malis JG, Zuidinga B, Borst A. A biophysical account of multiplication by a single neuron. Nature. 2022;603: 119–123. doi:10.1038/s41586-022-04428-3

18. Drews MS, Leonhardt A, Pirogova N, Richter FG, Schuetzenberger A, Braun L, et al. Dynamic signal compression for robust motion vision in flies. Curr Biol.. 2020;30: 209-221.e8. doi:10.1016/j.cub.2019.10.035

19. Matulis CA, Chen J, Gonzalez-Suarez AD, Behnia R, Clark DA. Heterogeneous temporal contrast adaptation in *Drosophila* direction-selective circuits. Curr Biol.. 2020;30: 222-236.e6. doi:10.1016/j.cub.2019.11.077

20. Pirogova N, Borst A. Contrast normalization affects response time-course of visual interneurons. PLOS ONE. 2023;18: e0285686. doi:10.1371/journal.pone.0285686